Boussinesq modeling of breaking waves: Description of turbulence

R. Briganti,[1] R. E. Musumeci,[2] G. Bellotti,[1] M. Brocchini,[3] and E. Foti[2]

Received 25 July 2003; revised 26 February 2004; accepted 31 March 2004; published 22 July 2004.

[1] Improved turbulent closures for use in fully nonlinear Boussinesq-type models are described here. The approach extends previous works in order to give a more flexible and accurate description of the turbulence due to a breaking wave. Turbulent stresses are handled by means of the Boussinesq hypothesis, and the eddy viscosity is assumed to vary over the water depth according to different laws. The model is described in detail, and its performances are evaluated both against available analytical solutions and against experimental data of regular waves breaking over a slope. The influence of the vertical structure of turbulence under a breaking wave is analyzed by means of four different vertical profiles of eddy viscosity; the differences in terms of hydrodynamic features are also discussed. Among the four selected profiles, two of them (the uniform one and that with uniform eddy viscosity over the top half of the water column which linearly decreases to zero over the lower half) give better overall performances when compared with experimental data concerning velocity profiles. *INDEX TERMS:* 4560 Oceanography: Physical: Surface waves and tides (1255); 4546 Oceanography: Physical: Nearshore processes; 4568 Oceanography: Physical: Turbulence, diffusion, and mixing processes; *KEYWORDS:* Boussinesq modeling, breaking waves, turbulence

Citation: Briganti, R., R. E. Musumeci, G. Bellotti, M. Brocchini, and E. Foti (2004), Boussinesq modeling of breaking waves: Description of turbulence, *J. Geophys. Res.*, *109*, C07015, doi:10.1029/2003JC002065.

1. Introduction

[2] The present study aims at improving the treatment of wave breaking in Boussinesq-type equations (BTEs). Although Boussinesq models can handle most of wave phenomena occurring in the nearshore (like refraction, diffraction, shoaling, frequency dispersion and nonlinear interaction) they cannot predict either where and when a wave breaks or, particularly, the hydrodynamic features of a breaking wave. In order to overcome the latter limit, in the last decade a number of approaches have been proposed (see, e.g., *Musumeci et al.* [2003] (hereinafter referred to as MSF) for a review). In the present work, on the basis of the method initially proposed by *Veeramony and Svendsen* [1999] (hereinafter referred to as VS), the fully nonlinear, wave breaking Boussinesq-type model (BTM) of MSF is taken as a starting point for analyzing the effects of turbulence description within the surf zone. The model of VS, which makes use of the roller approach, has been chosen since in it the effects of wave breaking are estimated from the knowledge of the vorticity structure inside the fluid (i.e., the rotationality of the fluid is accounted for). However, since the dynamics of vorticity and that of turbulence are strongly related to each other, the appropriate description of such mechanisms becomes a crucial point in modeling wave breaking with a BTM. As we aim at modeling spilling breakers by BTMs, which are most suited to represent the flow due to long waves over gently sloping beaches, knowledge of the structure of turbulence generated in quasi-steady breakers [see *Peregrine*, 1992] is fundamental to our analysis.

[3] The many difficulties in understanding the various aspects of wave-breaking often suggest to get quantitative information from flows similar to those occurring in spilling breakers but easier to handle from a theoretical and experimental point of view. Hence the analogy between a spilling breaker and a hydraulic jump [*Peregrine and Svendsen*, 1978] is often used. Quasi-steady breakers can be obtained with various experimental approaches: like the hydrofoil-induced breaker of *Duncan* [1981] or the gate-generated hydraulic jump of *Svendsen et al.* [2000]. Although these different approaches lead to turbulent flows sustained by different main flows, the main features are common. In particular it seems that turbulence spreads from a region characterized by high curvature of the water surface [*Lin and Rockwell*, 1995] known as the "toe of the breaker."

[4] Since turbulence develops because of an instability of a vortical flow, turbulence injection can only be clarified once the mechanisms for vorticity injection in a wave are known. Indeed, different mechanisms dominate as functions of the spatial scale [*Tulin*, 1996]. If surface tension is important, for water at scales of about 1cm, capillary waves

[1]Dipartimento di Scienze dell' Ingegneria Civile, Università degli Studi Roma Tre, Rome, Italy.
[2]Dipartimento di Ingegneria Civile e Ambientale, Università di Catania, Catania, Italy.
[3]Dipartimento di Ingegneria Ambientale, Università di Genova, Genova, Italy.

0148-0227/04/2003JC002065$09.00

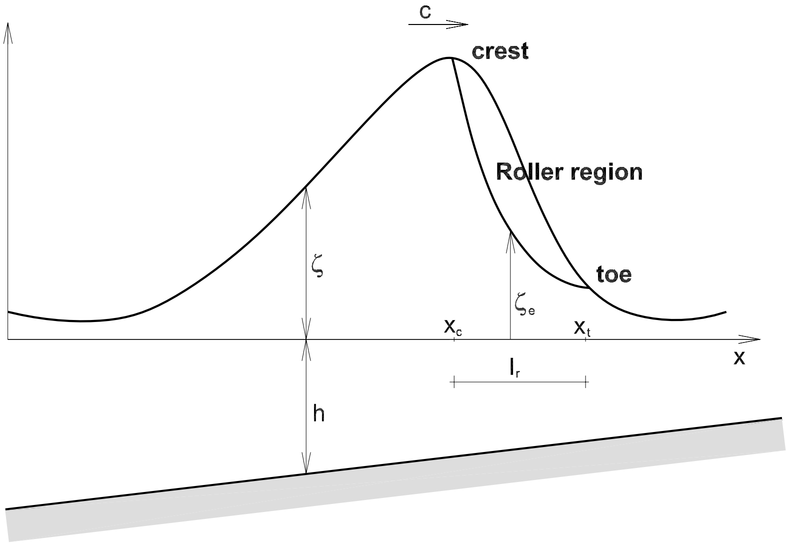

Figure 1. Sketch of flow characteristics and notation.

seem to be the main agent for vorticity injection [*Longuet-Higgins*, 1992; *Duncan et al.*, 1994]. On the contrary if surface tension is unimportant a small jet develops at the crest of the wave [*Tulin*, 1996] which, by impacting on the water surface, injects vorticity by a "surface reconnection mechanism" [e.g., *Hornung et al.*, 1995]. However, other mechanisms like viscous diffusion and surface shearing can be important [*Dabiri and Gharib*, 1997]. For a detailed analysis of these issues we refer the reader to the review of *Duncan* [2001]. Thus any numerical model which aims at reproducing the wave motion throughout the surf zone must take into account the aforementioned effects, even through a simplified approach.

[5] Among the most recent BTMs, the one proposed by VS, as mentioned, removes the assumption of irrotational flow, which is very often used, and regards the injection of vorticity due to the roller as the fundamental ingredient for a physically based description of the energy dissipation. VS used the similarity between the flow of a spilling breaker and that of a hydraulic jump to state boundary conditions describing vorticity injection at the lower edge of the roller. Hence a weakly nonlinear version of such a BTM, in which the breaking terms are derived directly through a decomposition of the velocity into a potential and a rotational part, was coupled with the vorticity transport equation (VTE) which, in turn, was used to evolve the horizontal component of the vorticity needed to compute the rotational contribution to the flow velocity. For closing the turbulence problem, VS assumed a simple eddy viscosity model, i.e., an uniform distribution over the depth. Such an assumption allowed to solve the VTE by means of an analytical approach.

[6] Although rather successful, the deliberately simple approach of VS is not flexible as it does not allow for a detailed description of the vertical structure of turbulence. Therefore in the present work the limiting hypothesis of uniform eddy viscosity has been removed and a numerical solution of the VTE is proposed, so that investigation of the effects of different eddy viscosity profiles is made possible. The model we discuss gives more flexibility in the choice of the shape of the eddy viscosity used to describe turbulence and allows for direct inspection of the various contributions to the transport of vorticity with the chosen turbulence closure. Moreover use of a refined grid in the solution of the VTE (by extending the regridding of MSF to our case) allows to describe energy dissipation by reducing to the bear minimum the use of stabilizing/dissipating mechanisms like numerical filtering.

[7] The paper is organized as follows. In section 2 the fully numerical solution is described and a sub-section is devoted to testing the numerical scheme for the VTE by means of an analytical solution. Numerical experiments of wave propagation over a slope are also described, and compared with two data sets coming from two suitable benchmark flows [*Hansen and Svendsen*, 1979; *Cox et al.*, 1995]. A parametric analysis on the role of various eddy viscosity profiles is finally carried out. A discussion on the many problems affecting energy dissipation in BTMs opens section 3 in which results are also discussed and an indication is given of the most suitable profiles to be used in computations. A brief conclusion rounds up the paper.

2. A Fully Numerical Solution

[8] In the present study a fully nonlinear BTM (VS; MSF) has been coupled with a numerical solver for the VTE. Details of the governing equations are given in Appendix A and a sketch of the flow variables is available in Figure 1. It is worth pointing out that the assumption of irrotational flow has been removed and thus the horizontal component of the velocity can be decomposed as:

$$u = u_p + u_r, \tag{1}$$

where u_p, representing the potential flow velocity, is equivalent to the velocity of typical potential flow formulations, while u_r, i.e., the rotational velocity component, is assumed to be only due to the vorticity caused by breaking, any contributions coming from the bottom boundary layer dynamics being neglected. Hence with this formulation extra terms appear in the momentum equation representing contributions to the momentum flux due to breaking. Such terms are only function of u_r and are thus referred to as "breaking terms" (terms inside the square bracket of the last line of equation (A2). It is worth pointing out that their computation requires knowledge of the rotational velocity which is a further unknown of the problem. In order to close the problem it is thus necessary to introduce one equation which relates u_r to the vorticity field due to breaking. Such an equation is given by the following relation, as in VS,

$$u_r \equiv \int_{-h}^{z} \omega dz' - \mu^2 \int_{-h}^{z} \int_{-h}^{z'} \int_{-h}^{z''} \omega_{,xx} dz''' dz'' dz' + O(\mu^4), \quad (2)$$

in which the vorticity ω is calculated by means of the VTE, which, in terms of the same nondimensional variables of the BTE reads:

$$\omega_{,t} + \delta u \omega_{,x} + \delta w \omega_{,z} = \nu_t \omega_{,zz} + 2\nu_{t_{,z}} \omega_{,z} + \nu_{t_{,zz}} \omega + O(\mu^2, h_x), \quad (3)$$

where w is the vertical velocity, $\mu = kh$, with k wave number and h water depth, is the dispersiveness parameter and $\delta = a/h$, with a wave amplitude, is the nonlinearity parameter. (Here the notation $(\cdot)_{,x}$ is used to represent partial differentiation.) In equation (3) the eddy viscosity ν_t is taken to be variable within the fluid, i.e., $\nu_t = \nu_t(x, z)$. In VS this quantity has been considered uniform over the water column, i.e., $\nu_t = \nu_t(x)$. The latter assumption allows for an analytic solution to be found which is determined by a suitable set of boundary conditions:

$$\omega(z = \zeta_e, t) = \omega_s(x, t), \qquad \omega(z = -h, t) = 0. \quad (4)$$

Hence in the following we refer to VS/MSF's solution as a semi-analytical solution: the VTE is solved analytically and its solution allows to compute the breaking terms appearing in the Boussinesq-type equations (A1) and (A2) which are solved numerically.

[9] Although the assumption of depth-independence of ν_t can be useful to derive VS's analytical solution, the turbulence structure of breaking waves is such that much of the turbulence generated at the free surface penetrates into the water body by vertical advection and diffusion [e.g., *Ting and Kirby*, 1996; *Chang and Liu*, 1999; *Melville et al.*, 2002]. It is, thus, clear that the assumption $\nu_{t_{,z}} = 0$ is theoretically rather crude and many experimental studies reveal the need for an adequate description of the vertical structure of ν_t [e.g., *Cox et al.*, 1995]. We here attempt at such a description which can only be possible if a suitable procedure is used to solve the VTE with $\nu_t = \nu_t(x, z)$. The first step is to introduce a change of variables (as used by VS) which allows for an easier treatment of the equation. The variables used in such a transformation read:

$$x = x, \quad t = t, \quad \sigma = \frac{h + z}{h + \delta\zeta_e}, \quad (5)$$

with ζ_e elevation of the lower edge of the roller. Such a change of coordinates allows for solution of the problem over a rectangular $(x, \sigma)-$domain. Since σ itself is a function of time and space, in the VTE new terms due to the coordinate variation in time and space appear. As in MSF, the final form of equation (3) in the $\sigma-$coordinates and accurate up to $O(\mu^2, h_x)$ reads:

$$\begin{aligned} &\frac{\partial\omega}{\partial t} - \delta\left[\frac{\sigma}{h + \delta\zeta_e}\frac{\partial\zeta_e}{\partial t}\right]\frac{\partial\omega}{\partial\sigma} + \delta u \frac{\partial\omega}{\partial x} - \delta\left[\frac{u\sigma}{h + \delta\zeta_e}\frac{\partial\zeta_e}{\partial x}\right] \\ &\cdot\frac{\partial\omega}{\partial\sigma} + \delta\left[\frac{w}{h + \delta\zeta_e}\right]\frac{\partial\omega}{\partial\sigma} = +\left[\frac{\nu_t}{(h + \delta\zeta_e)^2}\right]\frac{\partial^2\omega}{\partial\sigma^2} \\ &+ \left[\frac{\omega}{(h + \delta\zeta_e)^2}\right]\frac{\partial^2\nu_t}{\partial\sigma^2} + \left[\frac{1}{(h + \delta\zeta_e)^2}\frac{\partial\nu_t}{\partial\sigma}\right]\frac{\partial\omega}{\partial\sigma}, \end{aligned} \quad (6)$$

where, for the sake of clarity, we reverted to the standard notation for differentiation.

[10] The associated boundary conditions are given along iso-σ lines and read:

$$\omega(\sigma = 1, t) = \omega_s(x, t), \qquad \omega(\sigma = 0, t) = 0. \quad (7)$$

[11] Equation (6), together with boundary condition (7), can be coupled with the 1DH Boussinesq model equations in which the breaking terms are accounted for. In order to allow for a vertical variation of the turbulence (i.e., $\nu_t = \nu_t(x, z)$) we here use a numerical approach to solve equation (6) by means of a finite-difference technique. More specifically, an Adams-Bashforth-Moulton (ABM) [*Press et al.*, 1992] predictor-corrector method is used to integrate both the Boussinesq equations and the VTE.

2.1. Numerical Solver

[12] For the Boussinesq model the scheme is of third order in time at the predictor stage and of fourth order at the corrector stage. The ABM scheme which has been used to solve the VTE is of second order in time at the predictor stage and of third order at the corrector stage. The capability of the BTM to correctly describe the energy dissipation induced by wave breaking is largely dependent on the accuracy of the description of the vorticity magnitude under the breaking waves, hence the VTE solution requires an accurate description of the roller region i.e., of the region in which vorticity is produced. Since the length scale of the roller region is smaller than that of the waves, it is necessary to locally refine the computational grid. The use of a self-adaptive moving grid, which follows the roller region during the wave motion and refines the computation only where needed, seems rather suited to the purpose. The approach proposed in the work of MSF and R. Musumeci et al. (The flow in the surf zone: A fully nonlinear Boussinesq-type approach, submitted to *Coastal Engineering*, 2004, hereinafter referred to as Musumeci et al., submitted manuscript, 2004) has been extended to the present model. Starting from the knowledge of the wave crest and trough position (respectively x_c and x_t) at each time step, a moving subgrid is defined according these two relations:

$$\Delta x_g = \frac{x_t - x_c}{ng}, \quad \Delta x_{sg} = \frac{\Delta x_g}{ng}, \quad (8)$$

where Δx_g is the interval of the first subdivision of the subgrid while Δx_{sg} is the grid interval for the finer

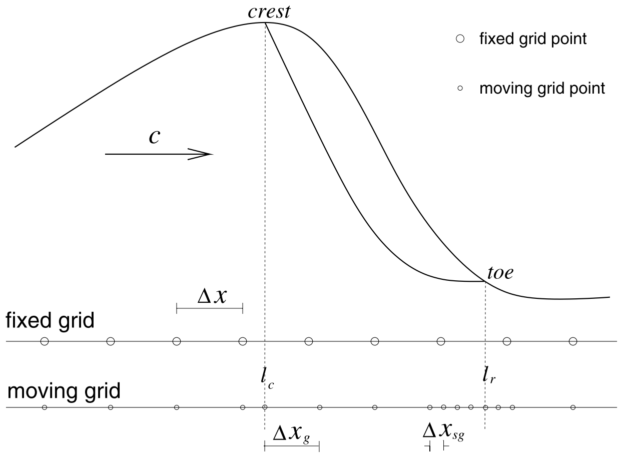

Figure 2. Sketch of the grid refinement in the roller region (adapted from MSF).

subdivision of the grid. The position x_g^i inside the roller is given by the relationship:

$$x_g^i = x_g^{i-1} + \begin{cases} \Delta x_g, & x_c \le x_g^{i-1} < x_t - \Delta x_g \\ \Delta x_{sg}, & x_t - \Delta x_g \le x_g^{i-1} < x_t. \end{cases} \tag{9}$$

The number of grid points inside the roller is, then, equal to 2*ng*. The moving grid coincides with the fixed one at each time step outside the roller. First-order derivatives both in *x* and *z* have been calculated using a "three points centered scheme" in the interior region while at the boundaries a one-sided scheme has been used. In the roller region such a scheme has been adapted to take into account the variability of the grid size. It is well known that use of finite-difference schemes with non-uniformly spaced grids increases the truncation error of the scheme, hence a gradual variation of the mesh is required. In this case, in order to describe the physics of the phenomenon, it is impossible to follow this approach. In order to increase the accuracy of the computation of the derivatives in *x*, two additional points spaced of Δx_{sg} have been added upstream the toe where the grid spacing shows the larger variation. Once the VTE is solved, u_r is computed on the moving grid and transferred on the fixed grid by means of a linear extrapolation. A sketch of the described grid is shown in Figure 2, further details on finite-difference approximations of the spatial derivatives and on the VTE scheme are reported in Appendix B and more details on the definition of the moving grid can be found in MSF. Since the stability condition of the Boussinesq model is different, in particular less restrictive, than the one of the VTE, a coupled integration in time should be run by using the small time step required for the VTE, hence drastically reducing the computational efficiency. To avoid such a problem a "mode-splitting technique" has been used to separate the time step of the Boussinesq model from the smaller one used in the VTE solver. A number of time steps of the VTE integration model (internal module) are carried out for each time step of the Boussinesq model (external module), it is generally sufficient to perform 4–5 internal time steps for each external one. Being retained as boundary conditions, the free surface elevation and the depth-averaged velocity are calculated by the external module, a data reconstruction by linear interpolation has been carried out in order to obtain values of such variables in the internal module. This technique is commonly employed in problems in which the free surface has to be solved together with a scalar quantity that diffuses in the fluid [*Simmons*, 1974; *Blumberg and Mellor*, 1987]. A sketch which illustrates the variables shared by the two modules is shown in Figure 3. The VTE module needs as input data the boundary value of ω (i.e., ω_s), the roller thickness ζ_s and the depth-averaged velocity

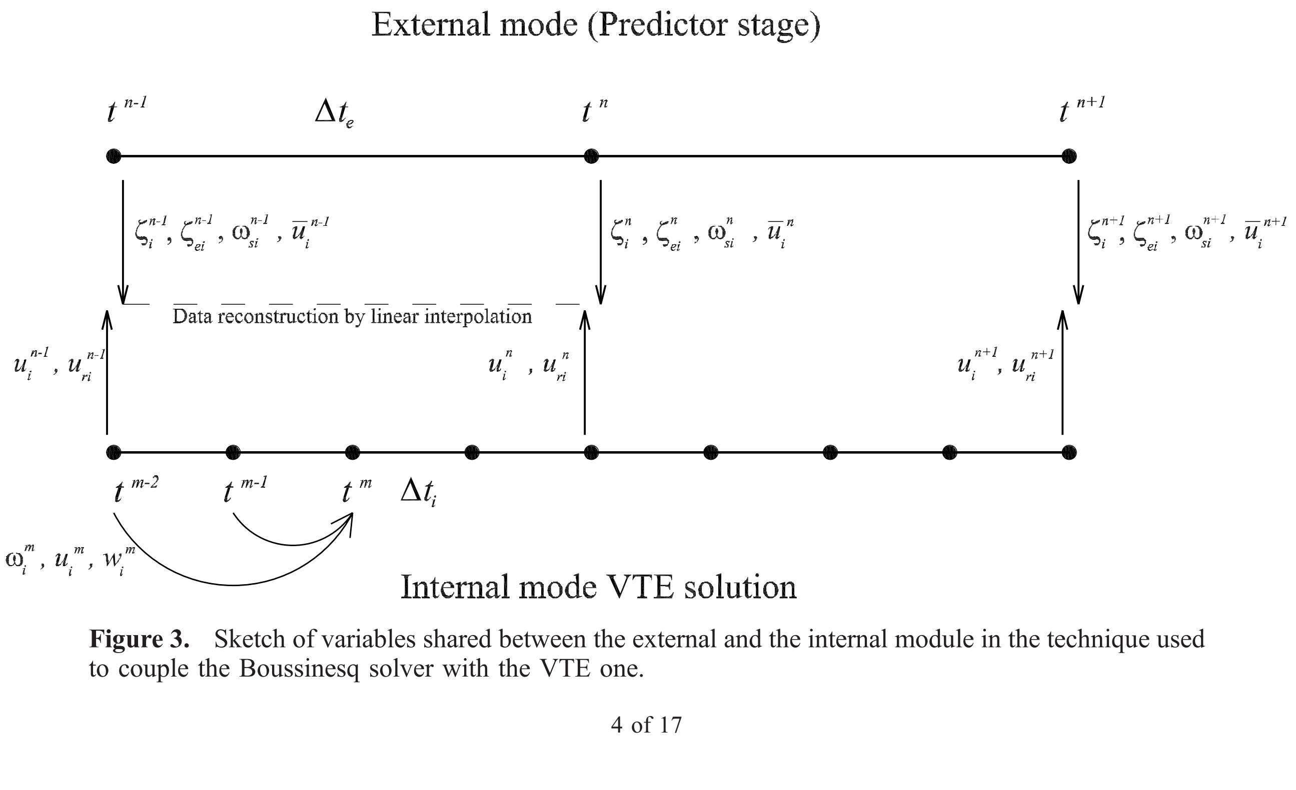

Figure 3. Sketch of variables shared between the external and the internal module in the technique used to couple the Boussinesq solver with the VTE one.

$\bar{u}$. Once rotational velocities have been computed, breaking terms are calculated in the external module and used to update the free surface and the depth-averaged velocity $\bar{u}$ by solving the BTE. A boundary condition for the vorticity has been proposed by VS through the following empirical relation, which is a best fit of the experimental data on hydraulic jumps of *Svendsen et al.* [2000]:

$$\omega_s = 15.75\left(1 - \frac{x - x_t}{l_r}\right)\left(1 - e^{-40\frac{x-x_t}{l_r}}\right), \tag{10}$$

where x_t is the position of the toe of the roller and l_r is the roller length. Equation (10) shows that the vorticity is maximum at the toe of the breaker. The roller thickness is also given by an empirical relation that reads:

$$\frac{\zeta_s}{h_2\sqrt{h_2/h_1}} = 0.78e^{-\frac{x'}{l_r}\left(\frac{x'}{l_r} - \frac{x'^2}{l_r}\right)}, \tag{11}$$

where h_2 and h_1 represent respectively the water depths upstream and downstream of the jump while $x' = -(x - x_t)$ (see also Figure 1).

[13] Finally, the local value of the velocity component u is estimated by the expression:

$$u = \bar{u}_p + \mu^2\left(h\bar{u}_p\right)_{,xx}\left(\frac{\Delta_1}{2} - z\right) + \frac{\mu^2}{2}\bar{u}_{p,xx}\left(\frac{\Delta_2}{3} - z^2\right) + u_r + \mathrm{O}\left(\mu^4\right), \tag{12}$$

where the rotational velocity is given by equation (2) and:

$$\Delta_1 = (\delta\zeta - h), \qquad \Delta_2 = \delta^2\zeta^2 - \delta\zeta h + h^2. \tag{13}$$

[14] The component w is obtained by using the continuity equation $u_{,x} + w_{,z} = 0$. Within the roller region the vorticity distribution cannot be numerically computed as the domain of integration is upper-bounded by the lower edge of the roller. Since the breaking terms $(\Delta M)_{,x}$, $(\Delta M_1)_{,x}$, D_{uw}, D_w and $(\Delta P)_{,xxt}$ contain contributions also coming from the roller area (as shown in Appendix A), the vorticity in that region is estimated by means of a linear extrapolation and by assuming $\omega = 0$ on the water surface. The same assumptions were also made by VS. Once ω has been computed, the above mentioned breaking terms can be evaluated.

[15] The eddy viscosity distribution over the water column $N(z)$ is assumed such that its maximum value is located at the water surface except at the roller where the maximum is located at the lower edge of the roller. This value is estimated by a mixing length hypothesis and ν_t given in the self-similar form:

$$\nu_t(z, x) = \nu_{t0}h(x)\sqrt{gh(x)}N(z), \tag{14}$$

where ν_{t0} typically assumes values in the range 0.01–0.04 [*Cox et al.*, 1995].

2.2. Validation of the VTE Solver

[16] Performances of the VTE solver have been tested by means of available analytical solutions for the evolution of a passive tracer in the case of linear advection and diffusion in an infinite domain. Since the vorticity is not a passive tracer these tests are mainly useful for evaluating the ability of the solver to adequately compute advection and diffusion. Other tests are proposed in the next section which are more suitable to evaluate the model performances in determining a physically correct solution.

[17] The problem considered here is:

$$C_{,t} + UC_{,x} = KC_{,xx}, \tag{15}$$

where C is the tracer concentration, U is the velocity of the flow (not influenced by the presence of the tracer) and K is the molecular diffusion coefficient of the tracer. The initial condition for the problem here considered is:

$$C(x, 0) = \delta_D(x), \tag{16}$$

i.e., the tracer has unitary concentration at the origin of the infinite domain at $t = 0$ (here δ_D indicates the Dirac's delta distribution). The analytical solution of this problem is the so-called "fundamental solution":

$$C(x, t) = \frac{1}{\sqrt{4\pi Kt}}e^{\frac{-(x-Ut)^2}{4Kt}}. \tag{17}$$

The proposed numerical scheme has been tested using $U = 1$ and $K = 1$. Figure 4 shows the comparison between the aforementioned analytical solution and the numerical solution obtained with the proposed numerical scheme. Results have been plotted at different values of $\sqrt{4Kt}$, i.e., $\sqrt{4Kt} = 2, 4, \ldots$ A very good agreement exists between the two solutions. We also compared the chosen ABM with the higher-order one used to solve the BTE. No differences could be found between the two methods at least within the machine round-off errors accuracy. Hence to increase the stability of the model without affecting the accuracy, the ABM scheme of second order at the predictor stage and of third order at the corrector stage has been used.

2.3. Comparison of the Fully Numerical Model (BTE + VTE) With Experimental Data

[18] The performances of the present model have been tested against two sets of experimental data from *Hansen and Svendsen* [1979] (hereinafter referred to as HS) and from *Cox et al.* [1995] and *Cox and Kobayashi* [1997] which share the same data set. The tests are mainly aimed at gaining information on the features of the numerical solution of the VTE by comparing the results with those obtained by means of VS/MSF's semi-analytical solution. We also try to assess the effects of turbulence description by assuming different depth-varying eddy viscosity profiles, i.e., different $N(z)$. Such an analysis has been carried out by making comparisons with the data of *Cox et al.* [1995], which are the most valuable, since velocity profiles are given along with other synthetic (wave-averaged) data like the wave height decay.

[19] The experimental studies in HS on the propagation of regular waves over a uniformly sloping beach have been carried out at the Technical University of Denmark. The flume was 0.6m wide, 32m long, the slope of the beach was 1:34.26 and its toe was 14.78m far from the wavemaker.

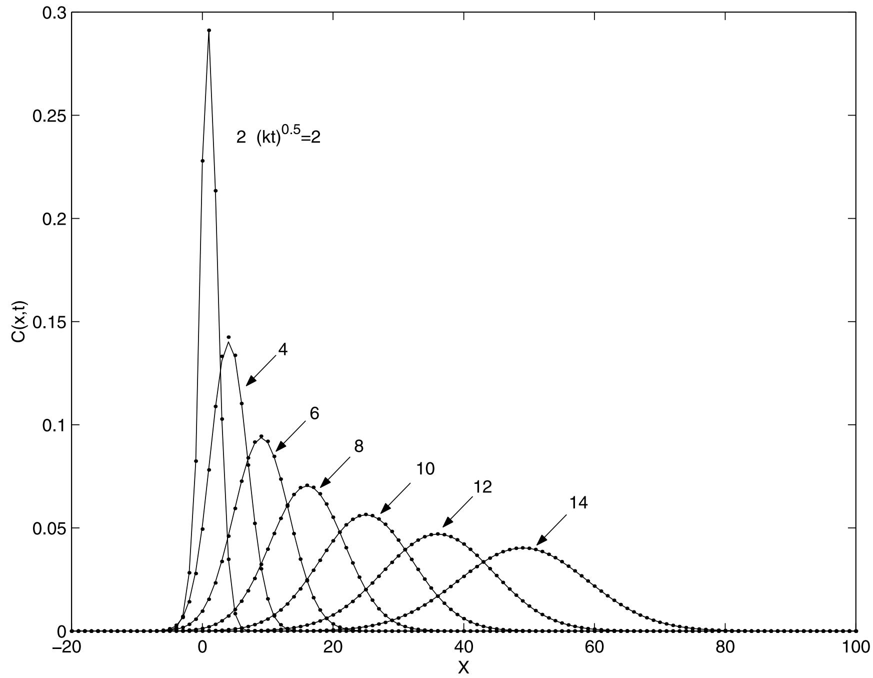

Figure 4. Comparison between the analytical solution of linear advection-diffusion of a passive tracer over an infinite domain (solid line) and the numerical solution of the same problem computed with the proposed scheme for the VTE (dots). Results have been shown at $\sqrt{4Kt}$ = 2, 4, 8, 10, 12.

Being the primary object of the experiments the evaluation of the wave height decay, wave heights were accurately measured by using a wave gauge mounted on a movable carriage. Unfortunately surface profile measurements are available only seaward of the breaking point, while no measurements were made of the flow velocities. Among the 18 wave conditions simulated in the experiments two cases of spilling breakers were chosen for the comparison. A summary of wave conditions of these two tests together with those concerning the other tests are shown in Table 1, in terms of the wave frequency f, the wave height H and the surf similarity parameter $\xi_0 = \tan(\alpha_s)/\sqrt{H/L_0}$, where α_s is the beach slope and L_0 is the wavelength close to the wavemaker. In Table 1 the flow parameters for all the considered data set are reported.

[20] The experimental setup of *Cox et al.* [1995] is quite similar to that described above. The experimental flume was 33 m long, 0.6 m wide and 1.5 m deep, the steepness of the sloping part was of 1:35. The bottom was made of concrete and it was made rough by gluing natural sand to the bottom (d_{50} = 1.0 mm). The water depth on the horizontal bottom was h_0 = 0.4 m. A schematic view of the experiment is given in Figure 5. Six measuring lines, $L1$, $L2$, $L3$, $L4$, $L5$, $L6$, were located along the slope. The position of the lines was chosen in order to have $L1$ in the shoaling region, $L2$ at the breaking point, $L3$ was in the transition region, $L4$, $L5$ and $L6$ were all in the inner surf zone (the position of the lines is given in Table 2). In correspondence of the six measuring lines, both surface elevation and flow velocities over the water column (significant only under the level of the wave trough) were measured. Cox and co-workers simulated only one wave condition obtaining spilling breakers. The same experimental setup has been used in the work of *Cox and Kobayashi* [1997] for measurement of the undertow current. The numerical flume used in the present study differs from the real one as it is not necessary to model the whole length of the depth-uniform region of the flume. The total length of the computational domain is of 18 m, where the horizontal bottom is 1 m long, with a water depth of h_0 = 0.4 m. At the onshore boundary a sponge layer is used, the onshore shelf is 5.65 m long with a depth of 0.04 m. In all the performed simulations cnoidal waves have been generated at the offshore boundary using a generating-absorbing boundary condition [*Van Dongeren and Svendsen*, 1997]. The breaking criterion has been introduced on the basis of a critical value for the surface slope.

[21] The first set of results shown here aims at comparing the fully numerical solution of the problem (VTE + Boussinesq) and the semi-analytical approach by VS/MSF (analytical VTE + numerical Boussinesq), using an uniform profile of eddy viscosity over the water column. All tests were run with spatial and temporal discretizations equivalent to those used in VS and MSF and best results were obtained by using a moving grid with ng = 5.

[22] Figure 6 shows the comparison between the wave heights along the flume obtained from the present model and from the experiments; the semi-analytical solution of

Table 1. Summary of the Wave Characteristics of the Performed Tests[a]

Test	f, Hz	H, m	ξ_0
HS test O	0.5	0.0375	0.38
HS test Q	0.4	0.04	0.44
Cox et al. [1995]	0.45	0.115	0.23

[a]Here f is input frequency, H is wave height, and ξ_0 is surf similarity parameter.

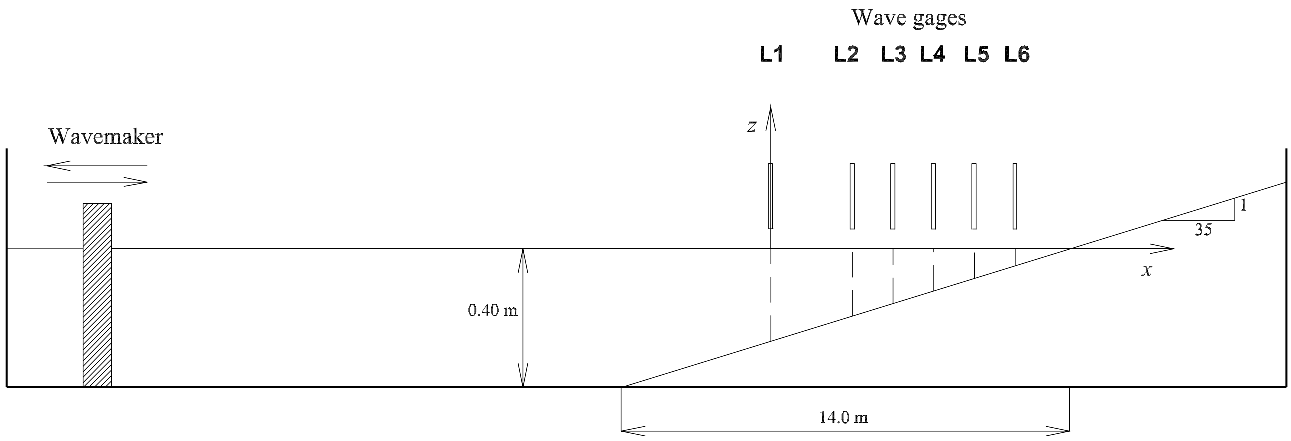

Figure 5. Experimental setup of *Cox et al.* [1995].

MSF's model is also reported for the sake of completeness. The wave height in the shoaling region is the result of the superposition of the incoming waves and those reflected off the beach. Only the latter contribution can be different in dependence of the approach (analytical or numerical) used to solve the VTE over the surf zone. For the case at hand this is negligible. Moreover, both models underestimate the wave height at breaking. In the transition region, both models predict almost the same wave height dissipation rate, which is different from that typical of the inner surf zone. The most important evidence which is brought up by these results is the difference between the models of VS/MSF and the present one in predicting the wave height distribution in the inner surf zone: the numerical solution of the VTE seems to give a lower dissipation. The source of this difference becomes more evident when looking at the velocity profiles predicted by the models and those coming from the experiments of *Cox et al.* [1995]. Also comparison with the wave height data of *Cox et al.* [1995] shows that the dissipation rate in the inner surf zone is higher in MSF's model than in the present one. (In both models waves begin to break in correspondence of $L3$, where, as shown in the experiments, breaking has already occurred). However, more useful is the comparison of the flow profiles.

[23] From the comparison of the evolution in time of the profiles of the vorticity (Figure 7, each panel shows surface profiles and vorticity profiles over a wave period at three chosen gauges: top panel L3, middle panel L4, bottom panel L6) it is clear that both models similarly represent the vorticity dynamics under the breaking wave. However, several remarkable differences require discussion. For example, even if vorticity downward penetration at the toe region is similar between the two models it should be noticed that the present model predicts a reduced vorticity penetration in the water body all along the wake of the roller. Moreover, the model of MSF predicts a rather intense vorticity upstream of the wave crest. Although the same fully nonlinear model of MSF is here used, a main difference arises in the solution of the VTE: here the solution is fully numerical while in MSF a numerical integration of an analytical solution is used. Hence assuming that such analytical solution is correct, two sources of differences are left. In order of increasing importance, the first cause of discrepancy can come the from the numerical quadrature method used in MSF, the second comes from the numerical scheme we use to solve the VTE. As already mentioned, we have used an ABM scheme which, however, is not the most suited for evolving shock-type solutions describing fronts associated to impulsive phenomena like the sudden vorticity injection here described. These differences largely influence the computation of the rotational velocities. Smaller abso-

Table 2. Position x and Depth h of the Measuring Lines in the Experimental Setup of *Cox et al.* [1995]

Line	x, m	h, m
$L1$	0.0	0.28
$L2$	2.4	0.211
$L3$	3.6	0.177
$L4$	4.8	0.143
$L5$	6.0	0.109
$L6$	7.2	0.0743

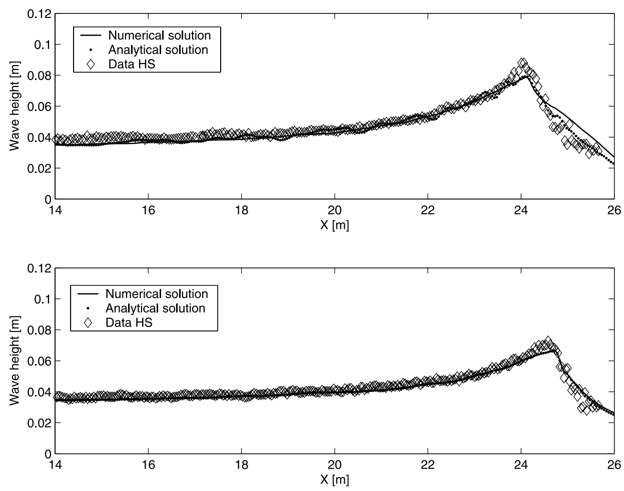

Figure 6. Wave height comparison among MSF's model, present model and data from HS ((top) test O; (bottom) test Q). Diamonds represent experimental results from HS, dots results from MSF's numerical simulations. Solid black line: present model. In both tests ν_{t0} = 0.01 and α_b = 30° have been used (see also VS and MSF).

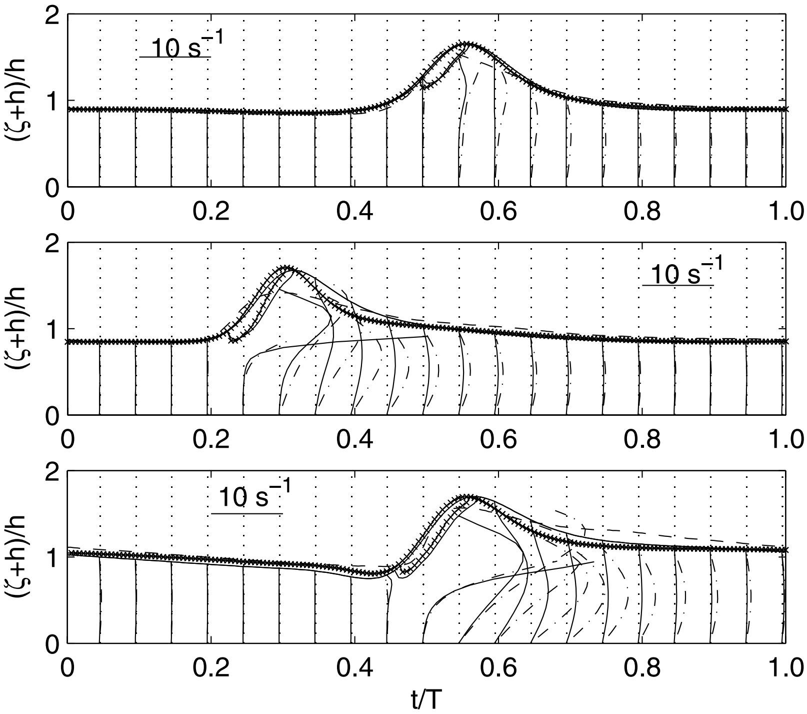

Figure 7. Time evolution of the vorticity profiles at three of the six locations ((top) L3, (middle) L4, (bottom) L6) of the gauges of *Cox et al.* [1995]. Surface profile: dashed line, experimental results; solid line, results from the present model using $N_0(z)$, ($x-$) line results from MSF's model. Vorticity profiles: solid line, results from the present model; dash-dotted line, results from MSF's model. ν_{t0} = 0.03 and α_b = 26°.

lute values of u_r are computed by means of the numerical solver of the VTE (Figure 8). However, from a qualitative point of view, the profiles of u_r computed from the analytical solution are, especially in the inner surf zone, characterized by stronger vertical gradients than both the numerical solutions and the experimental data.

[24] Comparison of the profiles of the total velocity u shows that this is overestimated by both models in correspondence of the crest (see Figure 9). Since MSF's solution predicts a rotational flow with strong vertical gradients, a similar feature can be seen in the total velocity, which differs from the measured profile, particularly in the upper part of the water column. However, as a result of the underestimate of energy dissipation, the present model predicts a larger velocity. Nevertheless, the profiles seem to be qualitatively similar to the measured ones. This is particularly true away from the wave crest where velocities predicted by the present solver, because of the smaller vorticity generation, fit better the experimental data than MSF's solution.

2.4. Sensitivity Analysis on Different Profiles $N(z)$

[25] In order to estimate the importance of the eddy viscosity distribution $N(z)$ over the water column, four possible test profiles have been chosen, which share the same maximum ν_{t0}. Figure 10 illustrates the shape of such profiles, $N_0(z)$ being the uniform profile for which results have already been shown in the previous section. The other three profiles are possible parameterizations of the turbulence structure all stemming from the observation that much of the vorticity and turbulence is introduced in the water body by the breaking wave near the surface. All the experimental observations available in the literature [e.g., *Peregrine and Svendsen*, 1978; *Okayasu et al.*, 1988; *Cox et al.*, 1995; *Svendsen et al.*, 2000] suggest that the eddy viscosity distribution over the upper half of the water column differs significantly from that in the lower half. Profiles with continuous derivative with respect to z (e.g., linear profile) have not been considered with the only exception of the uniform one which is used for comparison with MSF. Hence profiles $N_1(z)$ and $N_3(z)$ embody the assumption that turbulent stresses are non-zero only in the region of the water column directly influenced by the wave motion i.e., approximately the upper half of the normalized water column. This approach seems to be supported by experimental evidence of turbulence in hydraulic jumps [e.g., *Svendsen et al.*, 2000]. Profile $N_2(z)$ is the one similar to those reported by the experimental analysis of *Cox et al.* [1995] and also discussed in the work of *Deigaard et al.* [1991]. In summary, $N_0(z)$ and $N_2(z)$ are representative of turbulent stresses distributed over the whole water column while $N_1(z)$ and $N_3(z)$ represent turbulence localized in the upper part of the water column. It is obvious that the choice of the profiles is completely arbitrary and other possible profiles can be used. However, sensitivity analysis on these profiles can shed light on the structure of the most appropriate one to adequately represent the natural flow dynamics.

[26] Figures 11, 12, and 13 show the evolution in time respectively of the vorticity, of the rotational horizontal velocity and of the total horizontal velocity profiles as computed by the present model with both $N_2(z)$ and $N_3(z)$

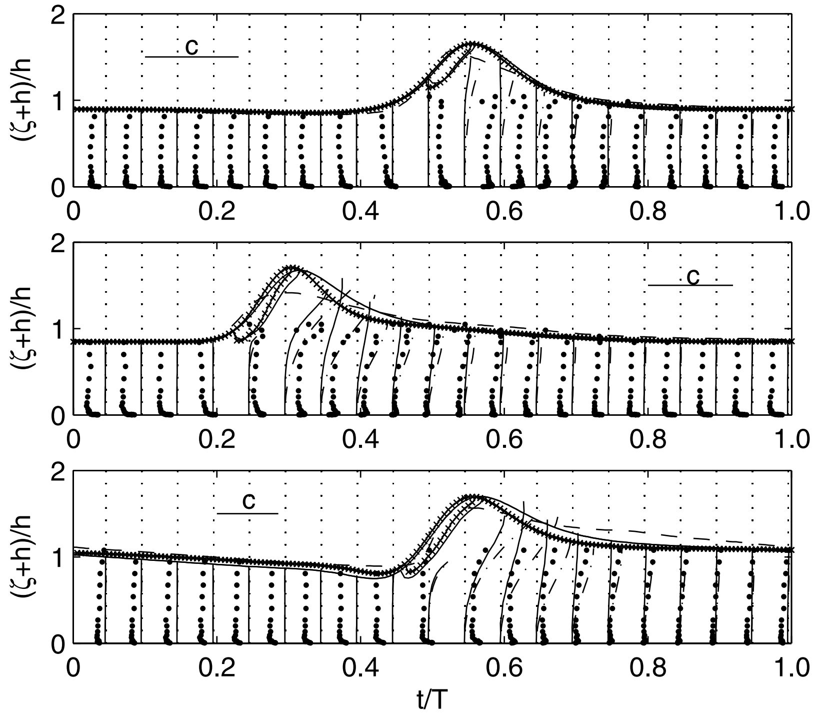

Figure 8. Time evolution of the rotational velocity at three of the six locations: (top) L3, (middle) L4, and (bottom) L6 of the gauges of *Cox et al.* [1995]. Surface profile: dashed line, experimental results; solid line, results from the present model using $N_0(z)$, $(x-)$ line results from MSF's model. Rotational velocity profiles: solid line, results from the present model; dash-dotted line, results from MSF's model. Dots represents the horizontal velocity measurements from LDV. c is the wave celerity computed as $\sqrt{gh}$.

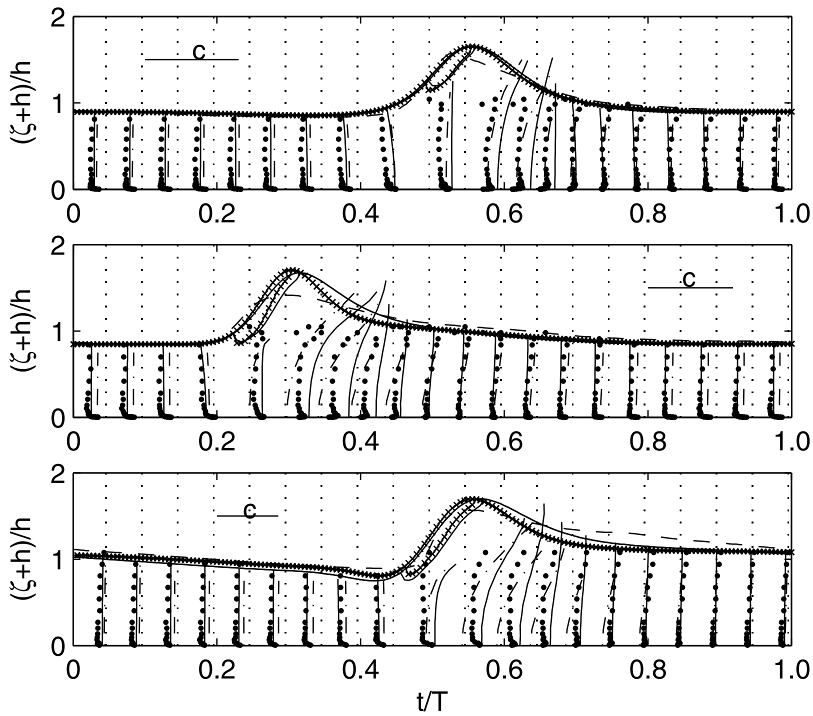

Figure 9. Time evolution of the total velocity at three of the six locations: (top) L3, (middle) L4, and (bottom) L6 of the gauges of *Cox et al.* [1995]. Surface profile: dashed line, experimental results; solid line, results from the present model using $N_0(z)$, $(x-)$ line results from MSF's model. Velocity profiles: solid line, results from the present model; dash-dotted line, results from MSF's model. Dots represents the horizontal velocity measurements from LDV. c is the wave celerity computed as $\sqrt{gh}$.

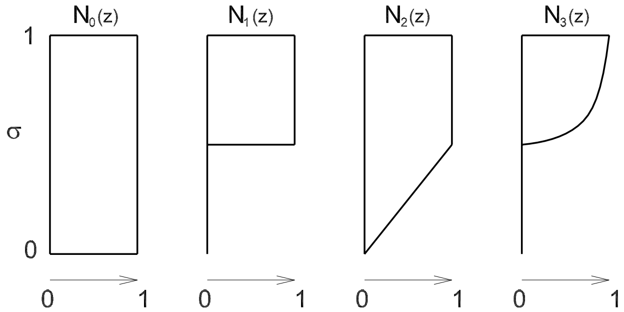

Figure 10. Eddy viscosity profiles chosen for the numerical simulations. The water column is normalized through the σ−coordinates transformation of equation (5).

and with ν_{t0} = 0.03. Note that, due to numerical reasons, even for $N_3(z)$ a non-zero eddy viscosity has been used over the lower half of the water column. However, its size was kept to 0.01 times the maximum value achieved by ν_t over the top half of the water column thus it can be regarded as uninflect for physical purposes.

[27] Weak vorticity is predicted by both $N_2(z)$ and $N_3(z)$ in the transition region ($L3$). However, in the inner surf zone ($L6$) more intense vorticity is predicted far from the roller region by means of $N_3(z)$ than by using $N_2(z)$ (see Figure 11): if the almost vanishing eddy viscosity in the lower half of the water column of $N_3(z)$ both inhibits vorticity diffusion and provides a limited vorticity dissipation. More details on vorticity evolution can be found in sections 3.2 and 3.3. Analysis of the velocity profiles reveals that differences among the various profiles of the rotational velocity (Figure 12) are more evident over the "wake region" (i.e., upstream of the crest) than over the crest area due to the aforementioned reasons. Hence at $L4$ and $L6$ the velocity away from the crest is better approximated by the simulations carried out with profile $N_2(z)$. When comparing the profiles of the total velocity (Figure 13) no major differences can be found between $N_2(z)$ and $N_3(z)$. The analysis also shows that the profile $N_1(z)$ (not reported here) leads to unreal spiky profiles of vorticity and velocity and, hence, cannot be considered as a good candidate for our modeling purposes. Such a behavior is clearly caused by the discontinuity of $N_1(z)$ at $(\zeta + h)/h = 0.5$. For the above reasons the profile $N_1(z)$ is not analyzed in more detail in the following.

[28] In order to quantitatively discuss the differences among the various models we have decided to measure the distance between the computed u_n^C and the experimental u_n^M velocity profiles (n being the discrete vertical level) in terms of the relative quadratic error:

$$\epsilon = \frac{\sum_{n=n_0}^{N} \left(u_n^C - u_n^M\right)^2}{\sum_{n=n_0}^{N} \left(u_n^M\right)^2}. \tag{18}$$

Note that the lowest level n_0 has been taken to coincide with the top of the bottom boundary layer, while N is the level of the water surface.

[29] We report relative errors of MSF's solution and of computations with $N_2(z)$ and with $N_3(z)$ in Figure 14. Inspection of the figure reveals that a rather large error characterizes the analytical solution over the "wake region" both within the transition region ($L3$) and over the surf zone

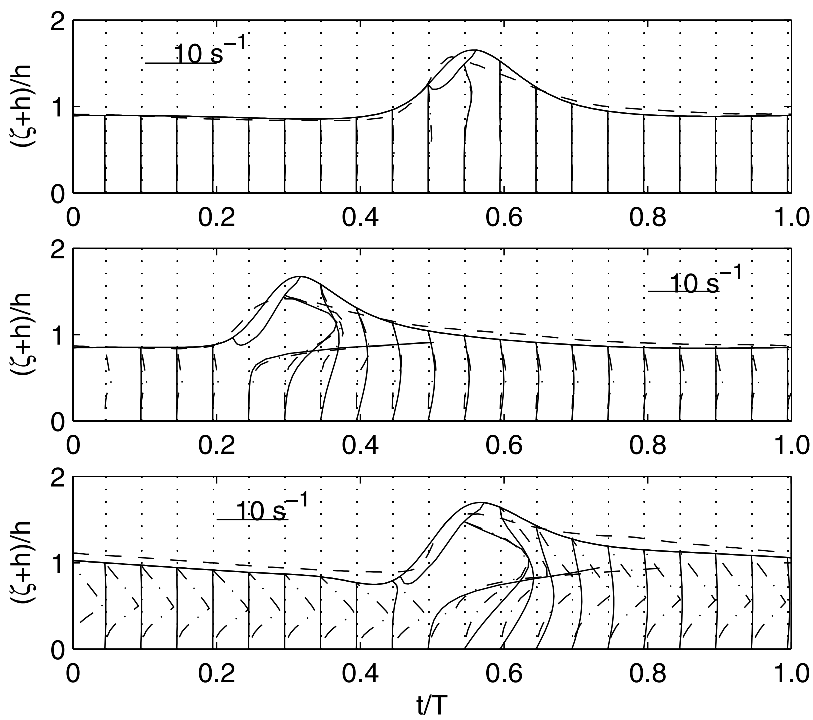

Figure 11. Time evolution of the vorticity profiles at three of the six locations (top panel L3, middle panel L4, bottom panel L6) of the gauges of *Cox et al.* [1995]. Solid line, $N_2(z)$ (with water surface and roller area); dashed-dotted line, $N_3(z)$. Dashed line surface profile of the experimental results of *Cox et al.* [1995].

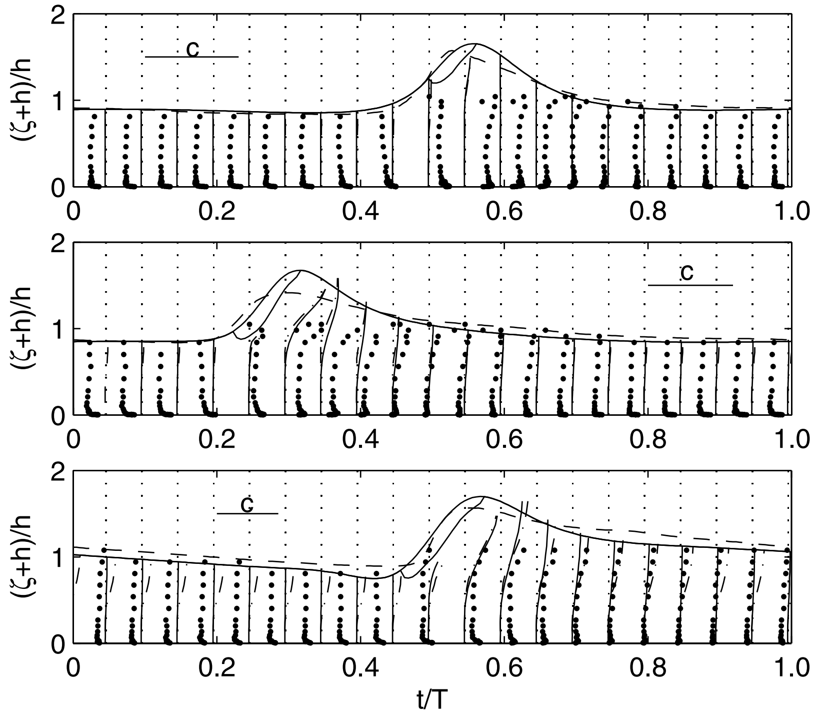

Figure 12. Time evolution of the rotational velocity at three of the six locations: (top) L3, (middle) L4, and (bottom) L6 of the gauges of *Cox et al.* [1995]. Solid line, $N_2(z)$ (with water surface and roller area); dashed-dotted line, $N_3(z)$. Dots and dashed line respectively give the rotational velocity and the surface profile of the experimental results of *Cox et al.* [1995]. c is the wave celerity computed as $\sqrt{gh}$.

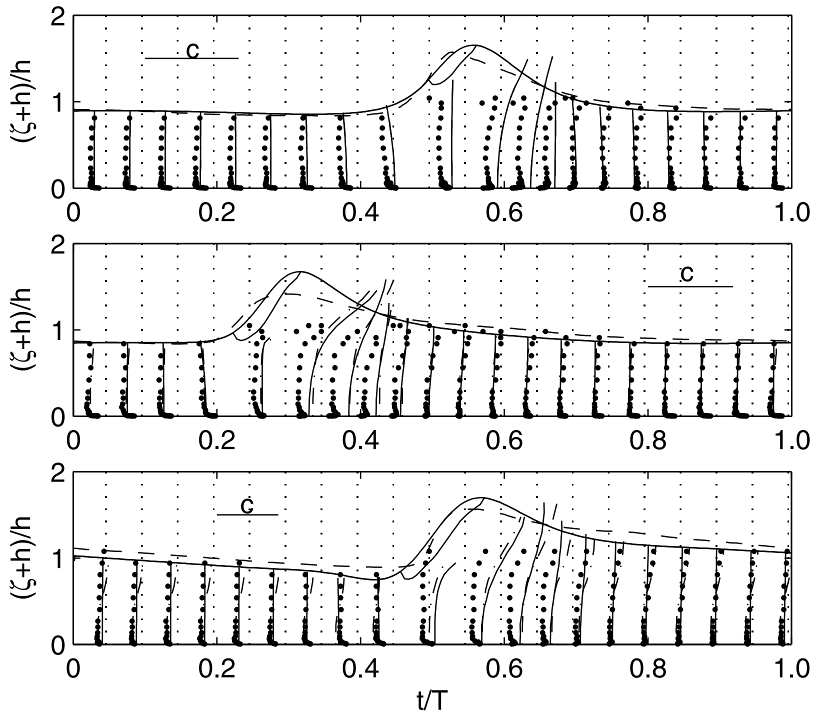

Figure 13. Time evolution of the total velocity at three of the six locations: (top) L3, (middle) L4, and (bottom) L6 of the gauges of *Cox et al.* [1995]. Solid line, $N_2(z)$ (with water surface and roller area); dashed-dotted line, $N_3(z)$. Dots and dashed line respectively give the rotational velocity and the surface profile of the experimental results of *Cox et al.* [1995]. c is the wave celerity computed as $\sqrt{gh}$.

Table 3. Summary of the Quadratic Error on the Velocity Profile for the Various Solvers Over the Surf Zone

Solver	L3	L4	L5	L6
Analytical	crest $\epsilon \approx 2$	crest $\epsilon \leq 1$	crest $\epsilon \approx 1$	crest $\epsilon \leq 3$
		wake $\epsilon \approx 5$	wake $\epsilon \approx 5$	wake $\epsilon \approx 2$
Numerical $N_0(z)$	crest $\epsilon \approx 2$	crest $\epsilon \leq 1$	crest $\epsilon \approx 1$	crest $\epsilon \leq 5$
		wake $\epsilon \leq 3$	wake $\epsilon \approx 1$	wake $\epsilon \approx 1$
Numerical $N_1(z)$	crest $\epsilon \approx 2$	crest $\epsilon \leq 1$	crest $\epsilon \approx 1$	crest $\epsilon \leq 2$
		wake $\epsilon \leq 5$	wake $\epsilon \leq 2$	wake $\epsilon \approx 2$
Numerical $N_2(z)$	crest $\epsilon \approx 2$	crest $\epsilon \approx 1$	crest $\epsilon \approx 1$	crest $\epsilon \leq 5$
		wake $\epsilon \approx 2$	wake $\epsilon \leq 1$	wake $\epsilon \approx 1$
Numerical $N_3(z)$	crest $\epsilon \approx 2$	crest $\epsilon \approx 1$	crest $\epsilon \approx 1$	crest $\epsilon \leq 2$
		wake $\epsilon \approx 4$	wake $\epsilon \leq 2$	wake $\epsilon \approx 3$

($L4$, $L6$). On the contrary good performances are achieved by the same method over the crest region. The overall best performances seem to be those of the numerical solution with either uniform ($N_0(z)$) or linear-uniform eddy viscosity ($N_2(z)$) while a worse comparison characterizes the numerical solution obtained with the parabolic profile $N_3(z)$. A synthetic description of the quadratic error for all the profiles considered over the surf zone is given in Table 3.

2.5. Undertow Profiles

[30] The "undertow current" plays a key role in the sediment transport processes within the nearshore region and, consequently, also in the morphodynamics of beach profiles. BTMs, in general, cannot predict the undertow profiles, because they do not consider the roller effect on the velocity field. The present model, being derived from MSF, drops the hypothesis of irrotational flow and takes into account the roller effects. Hence the undertow current may be evaluated according to the relation:

$$u_{undertow}(z) = u_{mean}(z) - \frac{\bar{Q}}{h_0 + \bar{\zeta}}, \tag{19}$$

in which the first term at the right hand side is the mean horizontal velocity (properly defined only for $-h < z < \zeta_{tr}$, ζ_{tr} being the surface elevation at the trough level), h_0 is the offshore water depth and ζ is the free surface elevation. The second term represents the correction for the sloshing in the experimental wave tank. $\bar{Q}$ is defined as:

$$\bar{Q} = \frac{1}{T} \int_{t}^{t+T} \int_{-h}^{\zeta_{tr}} u dz dt. \tag{20}$$

[31] Results of the models have been compared with the measurements of *Cox and Kobayashi* [1997] collected at six sections over the slope, which coincide with those of *Cox et al.* [1995]. Undertow profiles estimated with MSF's model and the present one with $N_0(z)$ and $N_2(z)$, are shown, for the three locations $L4$, $L5$ and $L6$ only, in Figure 15.

[32] The comparison of the profiles shows that results are similar even if the profiles at $L4$ and $L5$ seem to be better represented by the fully numerical solver which, with any chosen profiles of ν_t, gives vertically more uniform profiles than MSF's model. Quadratic errors have been summarized in Table 4. It is worth pointing out that the overall best performances have been obtained using the fully numerical solver with the $N_2(z)$ and $N_3(z)$ profiles. Even the profile $N_3(z)$ performs better than MSF's solution especially for the data of sections $L4$ and $L5$. In $L6$ performances are worse than those of the other models, this is probably due to the differences, already pointed out in the previous sections, in the velocity profiles. Another possible source of error is the incorrect use of the flow velocity at the top of the bottom boundary layer.

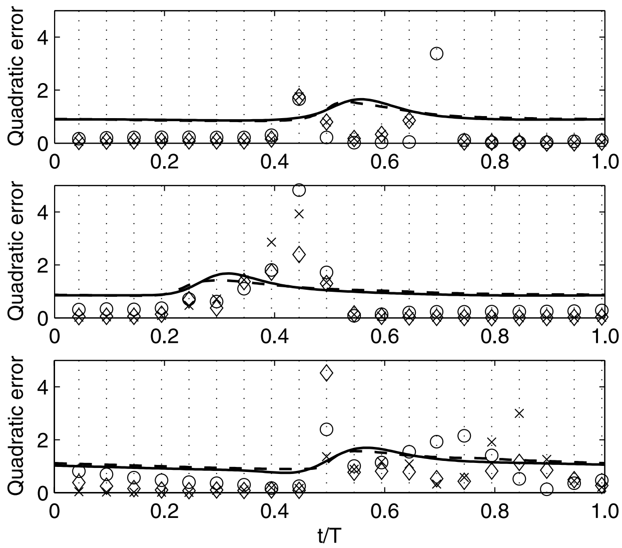

Figure 14. Quadratic error between the experimental and the computed velocity profiles over a wave period at three of the six locations: (top) L3, (middle) L4, and (bottom) L6 of the gauges of *Cox et al.* [1995]. Circles represent MSF's solution; diamonds represent numerical computations with $N_2(z)$; crosses represent computations with $N_3(z)$. The solid line and the dashed line give the experimental water surface from *Cox et al.* [1995] and the computed one with the numerical model using $N_2(z)$, respectively.

3. Discussion

[33] Some salient issues which have risen from the results shown in the previous sections are here discussed.

3.1. Energy Dissipation in BTMs

[34] One fundamental issue brought to our attention running the computations discussed in the previous section concerns the energy dissipation in BTMs. This is usually the sum of three main contributions: the theoretical contribution coming from the breaking-type terms (e.g., $(\Delta M)_{,x}$, $(\Delta P)_{,xxt}$, etc. in the present model), the intrinsic numerical contribu-

Table 4. Summary of the Quadratic Error on the Undertow for the Various Solvers Over the Surf Zone

Solver	L4	L5	L6
Analytical	0.1028	0.3670	0.0720
Numerical $N_0(z)$	0.0688	0.0237	0.0446
Numerical $N_1(z)$	0.0776	0.0123	0.0461
Numerical $N_2(z)$	0.0704	0.0269	0.0425
Numerical $N_3(z)$	0.0606	0.0214	0.1829

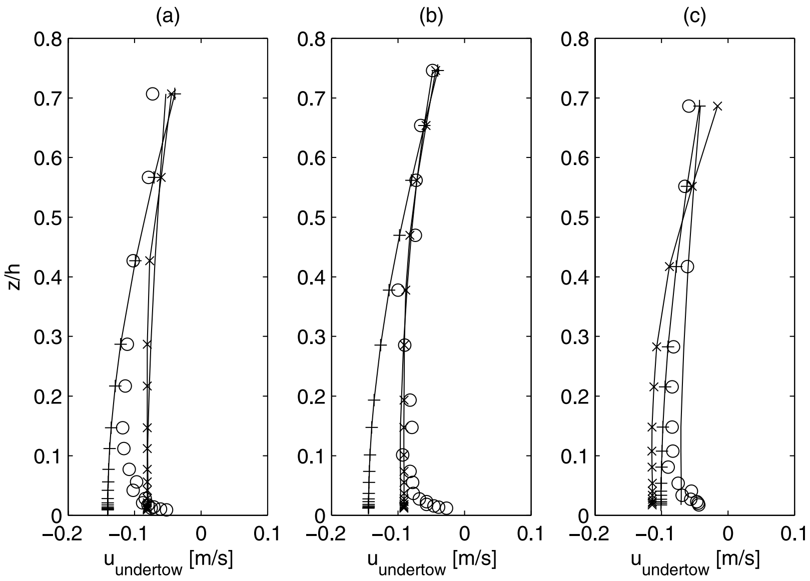

Figure 15. Undertow profiles: circles, data from *Cox and Kobayashi* [1997]; (+−) line, results from MSF's model; solid line, computation with $N_2(z)$; (x−) line, computation with $N_3(z)$. Panel (a) section L4, (b) section L5, (c) section L6.

tion coming from the numerical scheme in use and the extrinsic numerical contribution coming from any stabilizing mechanisms ad-hoc introduced to get stable solutions. In the case of most BTMs (like that of VS/MSF, of *Kirby et al.* [1998], etc.) the latter is represented by the so-called "Shapiro filter" [*Shapiro*, 1970] which is used to get rid of high-frequency oscillations. Note that, due to the dispersive nature of the BTM, the presence of breaking-type terms and to the characteristics of the ABM scheme, the Shapiro filter can become a powerful agent of energy dissipation. In fact frequency dispersion, highly promoted by the ABM scheme to the prejudice of nonlinear steepening (bore-like solutions are hard to get with the ABM), removes large amounts of energy from the fundamental frequencies in favor of higher frequencies falling in the range of operation of the Shapiro filter. Hence massive use of such filter leads to a substantial energy dissipation being caused by an extrinsic numerical mechanism capable of overshading the physical mechanism. An example of such effect is discussed in the work of Musumeci et al. (submitted manuscript, 2004) in which filtering was used within the surf zone at each computational time step (about 200 times each wave period). A more reasonable use of the filter in wave breaking simulations (i.e., a few times each wave period) is reported in the work of *Kirby et al.* [1998]. We here try to describe, as physically as possible, with the equations at hand, energy dissipation. Hence the use of the filter has been limited to 5–10 times each wave period and the efficiency of the physical dissipation (breaking) has been improved by means of the regridding described in section 2 [see also *Musumeci et al.*, 2003; MSF; *Briganti*, 2004; Musumeci et al., submitted manuscript, 2004]. All the above leads to question the value of the ABM scheme for this type of solutions. The way forward as discussed in the work of *Brocchini et al.* [2001] and *Bernetti et al.* [2003], is to devise a numerical approach which properly weights the two competing mechanisms of nonlinear steepening and frequency dispersion. This can be achieved, for example, by means of the "operator splitting method" [e.g., *Bernetti et al.*, 2003] which allows for the most suitable scheme to be used for each operator. In more detail shock-capturing, Godunov-type methods should be used for the nonlinear convective operator in conjunction with higher-order schemes for the dispersive operator.

3.2. Vorticity Transport Under Breaking Waves

[35] The results obtained so far can be used to briefly discuss the important issue of vorticity transport as described by the model. Since no detailed experimental data are available on the vorticity transport in breaking waves and since vorticity penetrates from the surface in the fluid body because of the same mechanisms that govern transport of the turbulent kinetic energy [e.g., *Melville et al.*, 2002] we discuss vorticity transport with reference to available experimental descriptions of the transport of turbulent kinetic energy [e.g., *Ting and Kirby*, 1996; *Chang and Liu*, 1999; *Melville et al.*, 2002].

[36] Figures 16 and 17 show the magnitude of different terms of the VTE as numerically computed by using the $N_2(z)$ profile both at $L3$, $L4$ and at $L6$. Figure 16 shows in detail the magnitude of terms over the crest region, while Figure 17 is focused on the wake region. Note the difference in the adopted plotting scales. Inspection of Figure 16 reveals that at the leading edge of the breaker vertical advection and vertical diffusion are positive over the whole water column (upward motion of the vorticity field) and larger in size than the horizontal advection which is negative. This means that vertical diffusion and advection dominate vorticity transport in that region. However, around the crest region horizontal advection becomes positive and larger than vertical transport contributions which have the same sign (negative near the surface) and, approximately the same size. A complicated transition between these two regimes is clearly shown by the data of $L6$. Moving from the toe to the crest vertical diffusion inverts sign (from

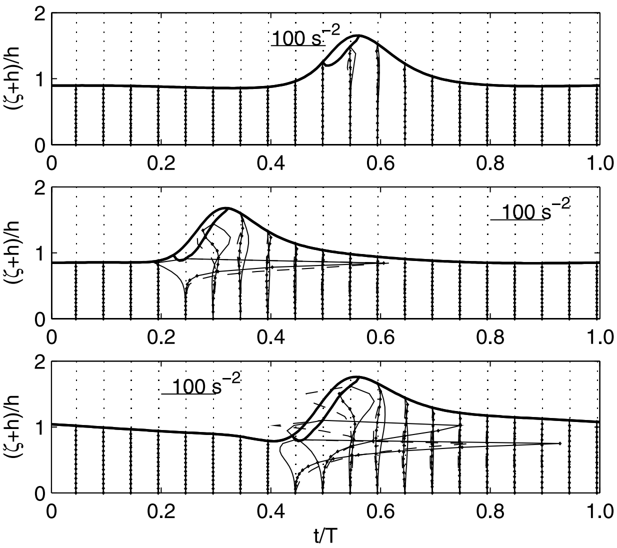

Figure 16. Illustration of some transport terms of the VTE as numerically calculated with the $N_2(z)$ profile at three of the six locations, (top) L3, (middle) L4, and (bottom) L6 of the gauges of *Cox et al.* [1995]. Horizontal advection (solid line), vertical advection (dots-) and vertical diffusion (dashed line) in the crest region.

positive to negative) near the surface before the vertical advection does and is characterized by a rather complex profile. At this section the leading term is the vertical advection which balances both vertical diffusion and horizontal advection. Moving closer to the wave crest also the vertical advection becomes negative and greatly decreases to become almost negligible with respect to the other two terms. Thus the effects of vertical advection dominates vorticity dynamics near the toe of the breaker but become negligible downstream of the wave crest. Over the so-called ''wake region'' (see Figure 17) vertical diffusion is negative and dominates meaning that the maximum of the vorticity profile moves downward into the water column. This dynamics of vorticity is in accordance with the interpretation given by *Ting and Kirby* [1996] who suggest that transport of turbulent kinetic energy within a spilling breaker is dominated by diffusion (or turbulent transport), vertical advection being important only near the surface. Finally, note that this scenario is substantially the same from the transition region ($L3$) to the inner surf zone ($L6$) as shown by the top and bottom panels of both figures.

3.3. A Suitable Profile for the Eddy Viscosity

[37] We here attempt at a choice of an eddy viscosity profile which, among the considered ones, seems more suitable to modeling purposes. The choice is guided both by the results already described and by interpretation of the dynamics associated with each profile (each profile corresponds to a different assumption on the turbulence structure).

[38] It is worth noticing that changes in eddy viscocity profiles mainly influence the profiles of the vorticity (Figure 11). It should be also pointed out that the profile $N_3(z)$, which prescribes a region with zero eddy viscosity, induces vorticity distributions rather different from those obtained with the uniform profile (especially over the ''wake region'') which has been shown to adequately model the flow dynamics. Over the ''roller region,'' which is interested by the beginning of vorticity transport in the fluid, differences seem to reduce due to the fact that vorticity is confined in the upper half of the water column, over which all profiles prescribe approximately the same value of eddy viscosity.

[39] As already seen the vertical extension of the vortical flow is governed both by advection (important in the roller between the toe of the breaker and the crest of the wave) and diffusion (dominating the ''wake region''). The latter is function of the size of ν_t, hence N_3 prescribes a negligible vertical diffusion over the lower half of the water column. However, a small eddy viscosity also induces a small dissipation of vorticity (better enstrophy) so that vorticity pushed down by vertical advection remains unrealistically intense also for long times. This is has already been shown in section 2.4 through the results in the lower panel of Figure 11.

[40] For the aforementioned reasons we think that the profile N_3 is less suitable than both N_0 and N_2 to describe the turbulence structure of breaking waves. We are now left with the choice between N_0, which has been tested both by VS/MSF and by us has showing good performances, and N_2. The latter, similar to N_0 over the top portion of the water column, seems the best candidate for modeling purposes as: (1) gives comparably good results of N_0 in terms of wave height decay; (2) gives moderately better results than N_0 in terms of velocity profile and undertow; (3) gives a sound description of the vorticity dynamics within a breaking wave; and (4) is supported by the accurate measurements of *Cox et al.* [1995].

3.4. A Suggestion for Further Improvements

[41] After the analysis of the above results we feel that the present model, independently on the profile N_i chosen for the eddy viscosity, does not predict very accurately the

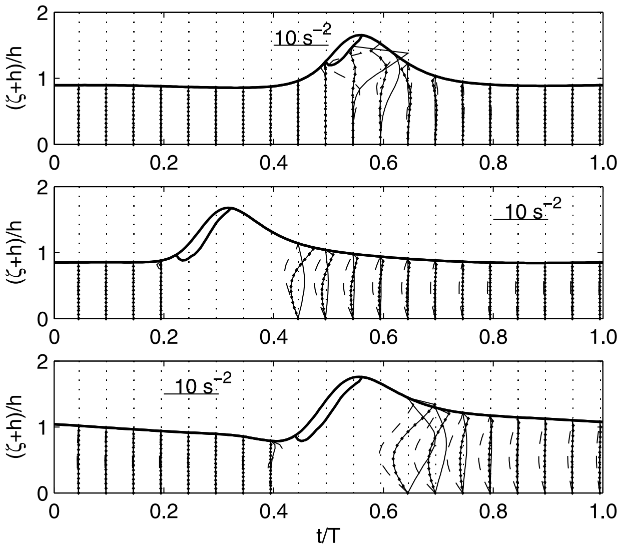

Figure 17. Illustration of some transport terms of the VTE as numerically calculated with the $N_2(z)$ profile at three of the six locations (top panel L3, middle panel L4, bottom panel L6) of the gauges of *Cox et al.* [1995]. Horizontal advection (solid line), vertical advection (diamonds) and vertical diffusion (dashed line) in the wake region. Note the difference in scale with respect to Figure 16.

experimental velocity profiles: indeed, the computed profiles are shifted with respect to the measured ones. This shift does not seem to depend only on the representation of the water surface as it is evident even when the computed water surface exactly matches the experimental one. We feel that the shift is linked to a poor prediction of the flow velocity just outside the bottom boundary layer u_b. In the present paper, as in VS/MSF, such a velocity is prescribed through the following approximate relationships,

$$u_{b,x} = \bar{u}_{p,x} + O(\mu^2), \qquad u_{b,xx} = \bar{u}_{p,xx} + O(\mu^2), \tag{21}$$

and has been used to obtain equation (12) in which u is dependent on $\bar{u}_p$ and u_r. The potential component $\bar{u}_p$ is calculated with the relation:

$$\bar{u}_p = \bar{u} - \bar{u}_r, \tag{22}$$

in which $\bar{u}$ is computed directly with the Boussinesq module and $\bar{u}_r$ is estimated from equation (2). It is clear that, since in the case of breaking $\bar{u}_p$ is computed as function of the vorticity generated by the breaking wave, also $u_{b,x}$ and $u_{b,xx}$, computed according to equation (21), are functions of the vorticity injected by breaking at the water surface. This seems a likely source of errors in the evaluation of equation (12) as u_b should be linked to the vorticity/turbulence generated within the bottom boundary layer with no major influences from the wave turbulence.

[42] In other words we think that the value of u_b appearing in the expression for the potential velocity

$$u_p = u_b + a(u_b, h)z + b(u_b, h)z^2 \tag{23}$$

should come from a model of the bottom boundary layer rather than from approximate analytical relationships as done here. Work is underway to define a suitable model of bottom boundary layer to be used in conjunction with the present Boussinesq model. Such model would also allow for a more flexible inclusion of either laminar or turbulent bottom boundary layer.

[43] We have also identified one second line of research with the aim of removing the present criterion for breaking which is based on the knowledge of the water surface slope and substitute it with a more physical and flexible criterion based on a comparison of the horizontal component of the flow velocity with the local wave speed. Finally, differences in the eddy viscosity distribution over the water column between the hydraulic jump described in the work of *Svendsen et al.* [2000] and the profile described for breaking waves in the work of *Cox et al.* [1995] have been found. We are currently evaluating such differences as depending on the different flow conditions (i.e., bore versus hydraulic jump). The main difference between the two flows comes from the unsteadiness of the bore and from the consequent different evolution of turbulence. Hence a detailed analysis of the transport properties of vorticity/turbulence in the flows is being performed.

4. Conclusions

[44] In the present study, VS/MSF's BTM for breaking waves in shallow waters has been extended to give a more flexible and accurate description of the effects of turbulence due to breaking waves. This has been achieved by allowing the eddy viscosity, used to represent turbulent stresses, to vary over the water column.

[45] A vertically varying eddy viscosity, in turn, requires a fully numerical solution of the VTE to be coupled with the Boussinesq solver. Hence a numerical solver based on the ABM predictor-corrector scheme has been implemented to solve the VTE. This scheme has been chosen as it allows for an adequate accuracy and for an optimal interlacing with the Boussinesq-type solver (the data-structure is basically the same). In order to improve the computational efficiency a "mode-splitting technique" has been used such that a number of time steps of the VTE integration model (internal module) are carried out for each time step of the Boussinesq model (external module). A self-adaptive, moving grid similar to that of MSF has been implemented in our solver. The high resolution of the roller dynamics allows for an efficient wave breaking energy dissipation and a reduced use of numerical filtering with respect to that typical of this sort of computations.

[46] The flow solutions of the fully numerical solver with uniform eddy viscosity profile have been compared both with the semi-analytical VS/MSF's solution and with experimental data. The data sets used for the comparison are those of *Hansen and Svendsen* [1979] and of *Cox et al.* [1995]. Analysis of the results reveals that the fully numerical solver injects in the flow less vorticity than that predicted by MSF's solution. Moreover, the vorticity seems to remain more confined in the upper half of the water column, never reaching the bottom as predicted by MSF's solution. As a consequence of the reduced energy decay we find that within the inner surf zone wave crests are less rounded and wave height decay is weaker. However, the profiles of the velocity (both rotational and total) seem to be qualitatively better predicted, especially away from the wave crests, than by MSF's model. The major discrepancy with the experimental data is caused by a shift, also characterizing MSF's solution, in the velocity profiles with respect to the experimental ones. We believe this shift is partly due to an incorrect prediction of the bottom boundary condition i.e., of the flow velocity at the top of the bottom boundary layer.

[47] We pushed forward our analysis to gain some knowledge on the most suitable profiles of eddy viscosity to be used for modeling. Hence a sensitivity analysis has been carried out aimed at comparing four possible profiles. We found that the uniform profile and that with uniform plus linearly decaying toward the bottom eddy viscosity give similar good overall comparisons in terms of wave height decay. Slightly better overall results have been obtained with the non-uniform profile which also gives a satisfactory description of the vorticity dynamics. Because of these results and supported by the experimental results of *Cox et al.* [1995] we find that such a profile is a good candidate for modeling breaking waves with the present BTM.

Appendix A: Equations of the Chosen BTE

[48] In VS/MSF, the Boussinesq equations have been derived by integrating the Reynolds equations over the

depth and by applying the kinematic and dynamic boundary conditions at the bottom and at the free surface. In particular (see Figure 1), using a cartesian reference frame (x, z) and by taking (u, w) as the horizontal and vertical velocity components respectively, the surface elevation, ζ, and the depth-averaged velocity, $\bar{u}$, can be used as the dependent variables of the BTE. These are made dimensionless with the following scales: the wave number k, the local water depth h and the wave amplitude a. The following equations are thus obtained which are characterized by two dimensionless parameter $\mu = kh$ (measuring the frequency dispersion) and $\delta = a/h$ (measuring the nonlinearities):

$$\zeta_{,t} + [\bar{u}(h+\delta\zeta)]_{,x} = 0 \tag{A1}$$

$$\begin{aligned}
&\bar{u}_{,t} + \delta\bar{u}\bar{u}_{,x} + \zeta_{,x} + \mu^2\left[\left(B - \frac{1}{3}\right)h^2\bar{u}_{,xxt} - \frac{1}{2}hh_{,xx}\bar{u}_{,t} - hh_{,x}\bar{u}_{,xt}\right] \\
&+ B\mu^2h^2\zeta_{,xxx} + \delta\mu^2\left[-\frac{1}{3}h^2\bar{u}\bar{u}_{,xxx} - h\zeta_{,x}\bar{u}_{,xt} + \frac{1}{3}h^2\bar{u}_{,x}\bar{u}_{,xx}\right. \\
&-\frac{2}{3}h\zeta\bar{u}_{,xxt} - \frac{3}{2}hh_{,xx}\bar{u}\bar{u}_{,x} - \frac{1}{2}hh_{,xxx}\bar{u}^2 - hh_{,x}\bar{u}\bar{u}_{,xx} - \zeta h_{,x}\bar{u}_{,xt} \\
&\left.- h_{,x}\zeta_{,x}\bar{u}_{,t} - \frac{1}{2}\zeta h_{,xx}\bar{u}_{,t} + Bh^2\left(\bar{u}\bar{u}_{,x}\right)_{,xx}\right] + \delta^2\mu^2\left[\frac{1}{6}\zeta^2\bar{u}_{,xxt}\right. \\
&- \frac{1}{3}h\zeta\bar{u}_{,x}\bar{u}_{,xx} - \frac{1}{3}h\bar{u}_{,xx}(\zeta\bar{u})_{,x} + h\left(\zeta\bar{u}_{,x}^2\right)_{,x} - \frac{1}{2}\left(\zeta^2\bar{u}_{,xt}\right)_{,x} \\
&- \frac{2}{3}h\left(\zeta\bar{u}\bar{u}_{,xx}\right)_{,x} - \zeta_{,x}h_{,xx}\bar{u}^2 - \zeta h_{,x}\bar{u}\bar{u}_{,xx} - \frac{1}{2}\zeta h_{,xxx}\bar{u}^2 - \frac{3}{2}\zeta h_{,xx}\bar{u}\bar{u}_{,x} \\
&\left.- \zeta_{,x}h_{,x}\bar{u}\bar{u}_{,x}\right] + \delta^3\mu^2\left[-\frac{1}{3}\zeta^2\bar{u}\bar{u}_{,xxx} - \zeta\zeta_{,x}\bar{u}\bar{u}_{,xx} + \zeta\zeta_{,x}\bar{u}_{,x}^2\right. \\
&\left.- \frac{1}{3}\zeta^2u_{,x}\bar{u}_{,xx}\right] + \left[\delta(\Delta M)_{,x} + \mu^2\left((\Delta P)_{,xxt} - D_s\right) + \delta\mu^2\left((\Delta M_1)_{,x}\right.\right. \\
&\left.\left. + D_w + D_{uw}\right)\right](h+\delta\zeta)^{-1} = 0,
\end{aligned} \tag{A2}$$

where the linear operator,

$$L = 1 + B\mu^2h^2\frac{\partial^2}{\partial x^2}, \tag{A3}$$

introduced by *Madsen et al.* [1991] to improve the dispersion properties has also been applied (the value of B is chosen so that the model's dispersive characteristics better mimic the linear theory in deep waters). In equations (A1) and (A2), the flow velocity is computed by differentiating the stream function ψ which, in turn, can be obtained by integrating in space the equation which defines ω in terms of ψ.

[49] The breaking terms read as:

$$\Delta P = -\int_{-h}^{\delta\zeta}\int_{z'}^{\delta\zeta}\int_{-h}^{z''}(u_r - \bar{u}_r)dz'''dz''dz' \tag{A4}$$

$$\Delta M = \int_{-h}^{\delta\zeta}\left(u_r^2 - \bar{u}^2\right)dz' \tag{A5}$$

$$\Delta M_1 = -\bar{u}_{p,xx}\int_{-h}^{\delta\zeta}\left(2hz' + z'^2\right)(u_r - \bar{u}_r)dz \tag{A6}$$

$$\begin{aligned}
D_w = \int_{-h}^{\delta\zeta}\frac{\partial}{\partial x}\left[\left(\int_{-h}^{z'}(u_r - \bar{u}_r)dz''\right)\right. \\
\left.\cdot\left(\frac{\partial}{\partial x}\int_{-h}^{z'}(2\bar{u} + u_r - \bar{u}_r)dz''\right)\right]dz'
\end{aligned} \tag{A7}$$

$$D_s = \int_{-h}^{\delta\zeta}\frac{\partial^2}{\partial x^2}\int_{z}^{\delta\zeta}\nu_t\frac{\partial u}{\partial z'}dz' \tag{A8}$$

$$\begin{aligned}
D_{uw} = \int_{-h}^{\delta\zeta}\frac{\partial^2}{\partial x^2}\int_{z'}^{\delta\zeta}\left[(u_r - \bar{u}_r)\frac{\partial}{\partial x}\int_{-h}^{z''}\bar{u}dz''' + (\bar{u} + u_r - \bar{u}_r)\right. \\
\left.\cdot\frac{\partial}{\partial x}\int_{-h}^{z''}(u_r - \bar{u}_r)dz'''\right]dz''dz'.
\end{aligned} \tag{A9}$$

[50] In particular, D_s is related to the shear stress inside the fluid, $(\Delta M)_{,x}$ and $(\Delta M_1)_{,x}$ give the excess of momentum flux due to the vertical variation of the rotational velocity, $(\Delta P)_{,xxt}$ is the contribution to the pressure due to the vertical motion, D_w is the excess of momentum due to the vertical motion and D_{uw} represents the interaction between the waves and the mean flow.

Appendix B: Finite Differences Schemes for the VTE

[51] As previously mentioned the VTE is solved by means of a third-order ABM scheme to step the model forward in time and a "three-point finite difference scheme" to evaluate the spatial derivatives. The VTE may be written using physical variables in a form that makes it convenient to apply the selected scheme:

$$\omega_t = W, \tag{B1}$$

where W contains quantities known from previous calculations:

$$\begin{aligned}
W = &\left[\frac{\sigma}{h+\zeta_e}\frac{\partial\zeta_e}{\partial t}\right]\frac{\partial\omega}{\partial\sigma} - \delta u\frac{\partial\omega}{\partial x} + \delta\left[\frac{u\sigma}{h+\zeta_e}\frac{\partial\zeta_e}{\partial x}\right]\frac{\partial\omega}{\partial\sigma} - \left[\frac{w}{h+\zeta_e}\right]\frac{\partial\omega}{\partial\sigma} \\
&+ \left[\frac{\nu_t}{(h+\zeta_e)^2}\right]\frac{\partial^2\omega}{\partial\sigma^2} + \left[\frac{\omega}{(h+\zeta_e)^2}\right]\frac{\partial^2\nu_t}{\partial\sigma^2} \\
&+ \left[\frac{1}{(h+\zeta_e)^2}\frac{\partial\nu_t}{\partial\sigma}\right]\frac{\partial\omega}{\partial\sigma}.
\end{aligned} \tag{B2}$$

[52] At the predictor stage the ABM time stepping scheme reads:

$$\omega_i^{n+1} = \omega_i^n + \frac{\Delta t}{2}\left[3W_i^n - W_i^{n-1}\right], \tag{B3}$$

while at the corrector stage it is:

$$\omega_i^{n+1} = \omega_i^n + \frac{\Delta t}{12}\left[5W_i^{n+1} + 8W_i^n - 1W_i^{n-1}\right]. \tag{B4}$$

[53] As it is known this scheme is accurate to O(Δt^2) at the predictor stage and up to O(Δt^3) at the corrector stage. W involves time derivative of the difference between the surface elevation and the roller thickness, which is calculated according to the relation:

$$\frac{\partial \zeta_e}{\partial t} + c\frac{\partial \zeta_e}{\partial x} = 0, \qquad \text{(B5)}$$

in which c represents the phase velocity of the wave crest.

[54] First-order spatial derivatives (along x and σ) are computed with a "three-point central differences scheme" in the interior region of the fluid. Since a nonuniform grid is used locally to solve the VTE, an expression of the derivatives evaluated in a point x_i which takes in account the unequal mesh size has to be used:

$$w_x \approx \frac{1}{2}\left(\frac{w(x_i+\Delta x_r) - w(x_i)}{\Delta x_r} + \frac{w(x_i) - w(x_i - \Delta x_l)}{\Delta x_l}\right) - \frac{\Delta x_r - \Delta x_l}{4}\frac{\partial^{2w}}{\partial x^2} - \frac{\partial^3 w}{\partial x^3}\frac{\Delta x_r^2 + \Delta x_l^2}{2\cdot 3!}, \qquad \text{(B6)}$$

where $\Delta x_r = x_{i+1} - x_i$ and $\Delta x_r = x_i - x_{i-1}$. Equation (B6) has been approximated with the first order of accuracy. Second-order spatial derivatives in the diffusive term are discretized using a "three-point scheme" in the interior of the fluid. A "four-point scheme" is used at the boundaries:

$$(\omega_{\sigma\sigma})_i = \frac{1}{\Delta\omega^2}[\omega_{i+1} - 2\omega_i + \omega_{i-1}], \quad i = 2,..,Nz-1 \qquad \text{(B7)}$$

$$(\omega_{\sigma\sigma})_1 = \frac{1}{\Delta\omega^2}[2\omega_1 - 5\omega_2 + 4\omega_3 - \omega_4] \qquad \text{(B8)}$$

$$(\omega_{\sigma\sigma})_{Nz} = \frac{1}{\Delta\omega^2}[2\omega_{Nz} - 5\omega_{Nz-1} + 4\omega_{Nz-2} - \omega_{Nz-3}]. \qquad \text{(B9)}$$

[55] **Acknowledgments.** Support from the European Union through the contract EVK3-2000-00038 (DELOS) and EVK3-CT-2001-00056 (SANDPIT), from the Italian M.I.U.R. (grant: "Influenza di vorticitá e turbolenza nella interazione dei corpi idrici con gli elementi al contorno e ripercussioni sulle progettazioni idrauliche") and from the G.N.D.C.I. of the C.N.R. (project: "Estimation and reduction of the risk in the coastal area") is acknowledged. I. A. Svendsen, N. Kobayashi, A. Okayasu, and D. T. Cox are thanked for making available to us their valuable data sets. We finally thank D. T. Cox and the two anonymous reviewers for their useful comments on this work.

References

Bernetti, R., E. F. Toro, and M. Brocchini (2003), An operator-splitting method for long waves, in *Long Waves Symposium, 30th IAHR Congress*, pp. 49–56, IAHR, Thessaloniki.

Blumberg, A. F., and G. L. Mellor (1987), A description of a three-dimensional coastal ocean circulation models, *Three-Dimensional Coastal Ocean Models*, *Coastal Estuarine Sci.*, vol. 4, edited by N. Heaps, pp. 1–16, AGU, Washington, D.C.

Briganti, R. (2004), Boussinesq modelling of breaking waves: Improvement of turbulence description, Ph.D. thesis, Univ. of Rome 3, Rome.

Brocchini, M., R. Bernetti, A. Mancinelli, and G. Albertini (2001), An efficient solver for nearshore flows based on the WAF method, *Coastal Eng.*, *43*, 105–129.

Chang, K. A., and P. L.-F. Liu (1999), Experimental investigation of turbulence generated by breaking waves in water of intermediate depths, *Phys. Fluids*, *11*, 3390–3400.

Cox, D. T., and N. Kobayashi (1997), Kinematic undertow model with logarithmic boundary layer, *J. Waterw. Port Coastal Ocean Eng.*, *123*, 354–360.

Cox, D. T., N. Kobayashi, and A. Okayasu (1995), Experimental and numerical modelling of surf-zone hydrodynamics, *Tech. Rep. CACR-95-07*, Cent. for Appl. Coastal Res., Univ. of Del., Newark.

Dabiri, D., and M. Gharib (1997), Experimental investigation of the vorticity generation within a spilling water wave, *J. Fluid Mech.*, *330*, 113–139.

Deigaard, R., P. Justesen, and J. Fredsoe (1991), Modelling of undertow by a one-equation turbulence model, *Coastal Eng.*, *15*, 459–474.

Duncan, J. H. (1981), An experimental investigation of breaking waves produced by a towed hydrofoil, *Proc. R. Soc. London A*, *377*, 331–348.

Duncan, J. H. (2001), Spilling breakers, *Annu. Rev. Fluid Mech.*, *33*, 519–547.

Duncan, J. H., V. Philomin, M. Beheres, and J. Kimmel (1994), The formation of spilling breaking water waves, *Phys. Fluids*, *6*, 2558–2560.

Hansen, J. B., and I. A. Svendsen (1979), Regular waves in shoaling water: Experimental data, *Tech. Rep., ISVA Ser., 21*, Tech. Univ. of Denmark, Denmark.

Hornung, H. G., C. Willert, and S. Turner (1995), The flow field downstream of a hydraulic jump, *J. Fluid Mech.*, *287*, 299–316.

Kirby, J. T., G. Wei, Q. Chen, A. B. Kennedy, and R. A. Dalrymple (1998), FUNWAVE 1.0: Fully nonlinear Boussinesq wave model documentation and users's manual, *Tech. Rep. CACR-98-06*, Cent. for Appl. Coastal Res., Univ. of Del., Newark.

Lin, J. C., and D. Rockwell (1995), Evolution of quasi-steady breaking wave, *J. Fluid Mech.*, *302*, 29–44.

Longuet-Higgins, M. S. (1992), Capillary rollers and bores, *J. Fluid Mech.*, *240*, 659–679.

Madsen, P. A., R. Murray, and O. R. Sørensen (1991), A new form of the Boussinesq equations with improved linear dispersive characteristics. Part 1, *Coastal Eng.*, *15*, 371–388.

Melville, W. K., F. Veron, and C. J. White (2002), The velocity field under breaking waves: Coherent structures and turbulence, *J. Fluid Mech.*, *454*, 203–233.

Musumeci, R., I. A. Svendsen, and E. Foti (2003), The flow in the surf zone: A fully nonlinear Boussinesq model for breaking waves, *Res. Rep. CACR-03-05*, Cent. for Appl. Coastal Res., Univ. of Del., Newark.

Okayasu, A., T. Shibayama, and K. Orikawa (1988), Vertical variation of undertow in the surf zone, in *Proceedings of the 21st International Conference on Coastal Engineering*, pp. 478–491, Am. Soc. Civil Eng., New York.

Peregrine, D. H. (1992), Mechanisms of water-wave breaking, in *Breaking Waves: IUTAM Symposium Sydney, Australia, 1991*, edited by M. L. Banner and R. H. J. Grimshaw, pp. 39–53, Springer-Verlag, New York.

Peregrine, D. H., and I. A. Svendsen (1978), Spilling breakers, bores and hydraulic jumps, *Proceedings of the 16th International Conference on Coastal Engineering*, pp. 540–550, Am. Soc. Civil Eng., New York.

Press, W. H., et al. (1992), *Numerical Recipes in FORTRAN: The Art of Scientific Computing*, 2nd ed., 963 pp., Cambridge Univ. Press, New York.

Shapiro, R. (1970), Smoothing, filtering and boundary effects, *Rev. Geophys. Space Phys.*, *8*, 359–387.

Simmons, T. J. (1974), Verification of numerical models of Lake Ontario: Part I. Circulation in spring and early summer, *J. Phys. Oceanogr.*, *4*, 507–523.

Svendsen, I. A., J. Veeramony, J. Bakunin, and J. Kirby (2000), The flow in weak turbulent hydraulic jumps, *J. Fluid. Mech.*, *418*, 25–57.

Ting, F. C. K., and J. T. Kirby (1996), Dynamics of surf-zone turbulence in a spilling breaker, *Coastal Eng.*, *27*, 131–160.

Tulin, M. P. (1996), Breaking of ocean waves and downshifting, in *Waves and Nonlinear Processes in Hydrodynamics*, edited by J. Grue, B. Gjevik, and J. E. Weber, pp. 177–190, Kluwer Acad., New York.

Van Dongeren, A. R., and I. A. Svendsen (1997), Absorbing-generating boundary condition for shallow water models, *J. Waterw. Port Coastal Ocean Eng.*, *123*, 303–313.

Veeramony, J., and I. A. Svendsen (1999), Modeling the flow in surf zone waves, *Res. Rep. CACR-99-04*, Cent. for Appl. Coastal Res., Univ. of Del., Newark.

R. Briganti and G. Bellotti, DSIC, Università degli Studi Roma Tre, Via Vito Volterra 62, I-00146 Roma, Italy. (briganti@uniroma3.it)

M. Brocchini, DIAM, Università di Genova, Via Montallegro 1, I-16145, Genova, Italy.

E. Foti and R. E. Musumeci, DICA, Università di Catania, Viale A. Doria 6, I-95125 Catania, Italy.